Photoionization of jet-cooled HI with coherent vacuum ultraviolet radiation: Evidence for Hund's case (e)

A. Mank, M. Drescher, T. Huth-Fehre,[a] N. Böwering, and U. Heinzmann
Universität Bielefeld, Fakultät für Physik, D-4800 Bielefeld 1, Germany

H. Lefebvre-Brion
Laboratoire de Photophysique Moléculaire, Bâtiment 213, Université de Paris-Sud, 91404 Orsay Cedex, France

(Received 25 February 1991; accepted 8 April 1991)

In the range of 83 500–89 200 cm^{-1}, the photoionization spectrum of HI is strongly influenced by autoionization of Rydberg series converging to the higher lying $^2\Pi_{1/2}$ component of the spin–orbit split $^2\Pi$ ionic ground state. The photoelectron yield spectrum, exhibiting the various autoionization processes, has been measured on a rotationally cooled sample ($T_{rot} \sim 13$ K), with a spectral resolution of the exciting vacuum ultraviolet radiation of 0.5 cm^{-1}. Using a multichannel quantum-defect theory treatment explicitly including rotation, we calculate spin–orbit and rotational autoionization fine structure in the spectrum. In order to find a qualitative agreement of theory and experiment, the Rydberg states of HI have to be described in terms of a transition in angular momentum coupling cases, going from Hund's case (c) to case (e).

I. INTRODUCTION

The study of molecular autoionization and competing processes has been of great interest for both experiment and theory in recent years. The advantages of the description in terms of a multichannel quantum-defect theory (MQDT) has been shown for various cases.[1] One of the molecules in these investigations was HI.[2] Since it is isoelectronic to the well studied xenon atom, comparisons in the autoionization behavior could be made.[3] A thorough study of the spin–orbit autoionization has been done by Eland and Berkowitz,[4] using photoionization mass spectrometry at moderate spectral resolution. They explained most features of the spectrum of HI and DI at room temperature in terms of five Rydberg series converging to the $^2\Pi_{1/2}$, $(v = 0)$ threshold and autoionizing into the $^2\Pi_{3/2}$, $(v = 0)$ continuum via spin–orbit interaction. No rotational structure could be detected.

In applying the MQDT to the problem of spin–orbit autoionization,[2] HI has been used as an example for the calculations. The first *ab initio* calculation did not include rotation, but predicted the overall intensity structure of the low resolution experiments to a certain degree. This calculation also gave results for the other dynamical parameters of the photoionization process, the angular asymmetry parameter β, the angle-integrated spin polarization, and the spin-polarization parameter ξ. They were put to a first test in a study of the angular asymmetry parameter β through angular resolved photoelectron spectroscopy using synchrotron radiation.[5] Within the limited resolution of this experiment, a certain agreement was found.

All these studies were restricted by lack of resolution in the exciting radiation. The development of vacuum ultraviolet (vuv) radiation sources utilizing resonant sum-frequency mixing of pulsed dye-laser radiation[6] made studies possible where the molecular rotation is resolved. In the first experiments, the rotationally resolved photoelectron yield spectrum of HI at room temperature were studied.[7,8] The coarse features of the data could be assigned to Rydberg series as in the earlier study,[4] but due to the higher resolution eight series were found. Rotational structure was clearly visible, but all attempts to assign rotational progressions gave ambiguous and inconclusive results. First experiments on a rotationally cooled sample[8] showed significant differences to the results at 300 K; the agreement with the rotationless theory[2] was still only modest. Studies of the angular asymmetry parameter β at different rotational temperatures[9,10] with narrow band vuv radiation provided no new insights for the rotational assignments.

In a more detailed study of the Rydberg member $n = 6$ at a rotational temperature of 13 K, not only the photoelectron yield, but also the angle-integrated photoelectron spin polarization has been measured using circularly polarized radiation ("Fano effect"). The intensity data could be fitted to a simple model, thereby assigning the observed rotational structure in the frame of Hund's case (c).[11] The angle-integrated photoelectron spin polarization was found to exhibit rotational structure, too. However, the results of the spin-polarization measurement and the assignment gave rise to open questions regarding the validity of pure Hund's case (c) coupling in this spectral region. For high Rydberg members the uncoupling of the total electronic angular momentum from the molecular axis could lead to a transition to Hund's case (e) coupling.[12] A similar effect occurs in the case of rotational autoionization in H_2, where the change goes from coupling case (b) to case (d).[13] Interest in Hund's case (e) has been stimulated by other experimental results, as well.[14]

In order to come to a more complete understanding of

[a] Present address: SRI International, Menlo Park, California 94025.

 0021-9606/91/151676-12$03.00

the spin–orbit autoionization process in HI, the photoelectron yield spectrum between the $^2\Pi$ ionic thresholds has been measured with high resolution at a rotational temperature of 13 K. In this paper, these experimental results are presented and an analysis is given in terms of a transition of angular momentum coupling from Hund's case (c) to case (e). The corresponding calculations reported here for the first time are based on an *ab initio* MQDT formalism including rotation.

In a different approach, the problem of the rotationally resolved molecular photoionization spectrum has been discussed implicitly in a pure Hund's case (e) approximation.[15] This theory has been applied to HI,[16] including spin–orbit autoionization, but neglecting rotational autoionization. These results still lack agreement with experiment, though they seem to fit better than the results without rotation.

II. EXPERIMENTAL

The experimental setup used to record the highly resolved photoelectron yield spectra in the energy region from 83 500 to 89 200 cm^{-1} has been described in detail elsewhere.[7,11,17] Briefly, it consists of a narrow band vuv source of high spectral brightness ($\Delta\tilde{\nu}\sim 0.5$ cm^{-1}, $I\sim 10^{10}$ $h\nu$/pulse at 11 Hz repetition rate) employing resonant sum-frequency mixing of pulsed dye-laser radiation in mercury vapor.[6] In order to simplify the spectrum, the target gas was prepared at a rotational temperature of ~ 13 K,[11] using a pulsed nozzle for a supersonic expansion. At this temperature, only two rotational levels of the ground state are populated significantly ($J''=0$: 56%; $J''=1$: 40%; $J''=2$: $<4\%$). Most of the electronic transitions in this energy region are of the type $^1\Pi\leftarrow{}^1\Sigma$. Weighting the relative transition moments of different rotational lines by appropriate Hönl–London factors leads to approximate relative intensities of $R(0):R(1):Q(1)$ as 0.28:0.1:0.1, respectively. The rotational bands are dominated by the $R(0)$ transitions. Recording the autoionization spectrum at this low rotational temperature for the entire energy region between the $^2\Pi$ ionic thresholds should enable an analysis of the observed structure which is easier to perform than for the case of congested spectra at 300 K rotational temperature.

The photoelectrons are collected in an electrostatic field[18] regardless of their kinetic energy and direction of emission. The field strength in the target region is below 15 V/cm; reducing the field by 1 order of magnitude resulted in no changes in the data. Except in the region below the first ionization threshold at 83 720 cm^{-1}, where we find structure that could be attributed to field ionization, effects from the electric field in the target region can be neglected. The experimental results for the total photoionization cross section were recorded in sections, each with a length of approximately 150 cm^{-1}. The scans were reproduced at least twice, the results were added to give relative statistical errors of less than 1%. Special care was taken in connecting these sections to the full spectrum. The absolute error in the relative peak heights for photon energies between 84 500 and 89 200 cm^{-1} is estimated to be less than 20%. Below 84 500 cm^{-1}, the possible error is considerably larger, but still less than 40%, due to problems with the infrared dyes used in the wavelength scanning dye laser. The reproducibility of the relative peak heights of neighboring structures is as good as the statistical errors. The radiation wave number is calibrated to an absolute accuracy of better than 0.5 cm^{-1} by recording spectra of laser-induced fluorescence in an iodine cell and opto-galvanic spectra in a Ne-filled hallow-cathode lamp for the visible laser outputs.

III. RESULTS

The experimental results, consisting of roughly 10 000 data points, are presented in Fig. 1. The dominant features can be attributed to spin–orbit autoionization into the $^2\Pi_{3/2}$, $(v=0)$ continuum of Rydberg series converging to the $^2\Pi_{1/2}$, $(v=0)$ ionic state. Furthermore, additional structure is superimposed due to vibrational autoionization of Rydberg series converging to the $^2\Pi_{3/2}$, $(v=1)$ ionic state at 85 858 cm^{-1} (Ref. 19), and of Rydberg series converging to the $^2\Pi_{1/2}$, $(v=1)$ ionic state and autoionizing via spin–orbit interaction into the $^2\Pi_{3/2}$, $(v=1)$ channel.[5,17] The photoelectrons of the latter series occur at different kinetic energies as can be seen from constant ionic state measurements with an electron spectrometer.[10] In this paper, we will discuss only Rydberg series converging to $^2\Pi_{1/2}$, $(v=0)$.

The fine structure in the experimental spectrum is attributed to transitions from a rotational level of the ground state to a distinct rotational level of the autoionizing Rydberg state. The term values of the members of a Rydberg series can be described as

$$T_i = \mathrm{IP} - \frac{R_{\mathrm{HI}}}{(n-\mu_i)^2} \tag{1}$$

(see, e.g., Ref. 20) where T_i is the term value, IP the ionization potential, and μ_i the quantum defect, which is different for each series. R_{HI}, the Rydberg constant for HI can be derived from the Rydberg constant R_∞ by employing the mass correction. The strongest transitions observed in the spectrum should be denoted as $R(0)$, since this is the dominating transition in each rotational band.

In comparing different members of the Rydberg series, one should keep in mind that the widths of the resonances scale as n^{-3}. For example, the $R(0)$ line of the $\pi^3 ns\sigma{}^1\Pi_1$ state has a width of 9.0 cm^{-1} at $n=6$.[11] Using the formulas given in Ref. 2, the width at $n=16$ can be calculated to be 0.34 cm^{-1}. Consequently, at high values of n, these levels will not be resolved with the spectral width of our light source. Only the resonances which appear as broad peaks in the lower Rydberg orders can be observed at very high n.

If the molecule HI can be described in one angular momentum coupling case exclusively, the quantum defects μ_i should be only weakly energy dependent and become independent of energy for high n. In this case, the values of the ionization potential and the different quantum defects μ_i can be extracted by fitting the experimental peak positions to Eq. (1). We used a nonlinear least-squares fitting procedure

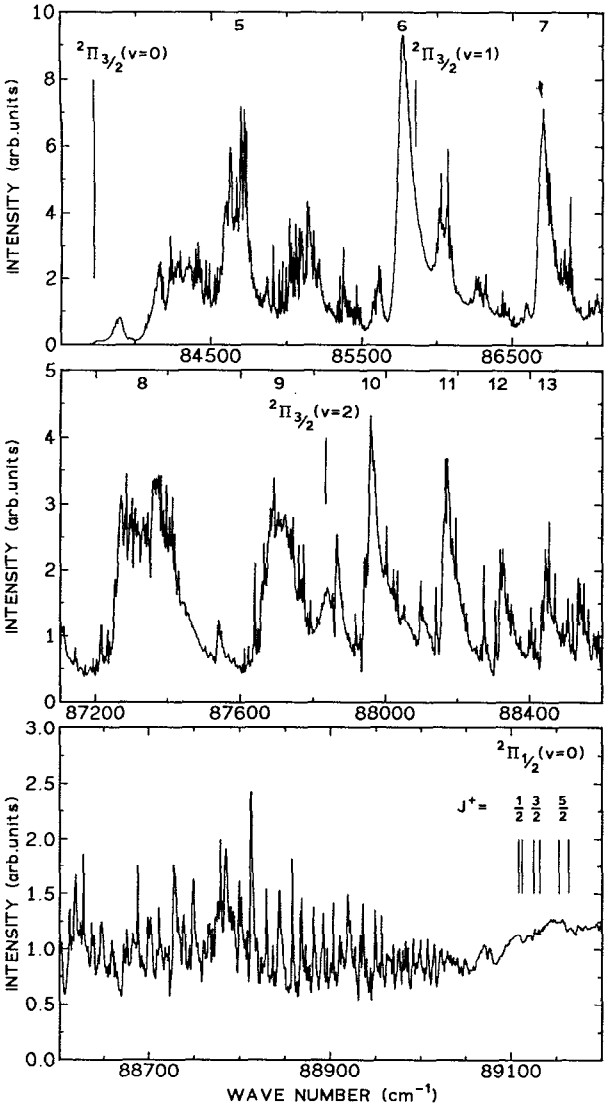

FIG. 1. Experimental results for the total photoionization cross section. The spectral width of the exciting vuv radiation is $\Delta\bar{\nu} < 0.5\ cm^{-1}$, the rotational temperature of the molecular beam 13 K. Note that the ordinates have been enlarged at higher excitation energies in order to reproduce the fine structure of the results more clearly. The different members of the Rydberg series are given by their integer values for $n = 5$ to $n = 13$. Furthermore, the vibrational levels $v = 0, 1, 2$ of the $^2\Pi_{3/2}$ substate and the different rotational levels $J^+ = 1/2, 3/2, 5/2$ of the $^2\Pi_{1/2}$ substate with their splitting into the *e*- and *f*-parity components are indicated.

employing the routines given in Ref. 21 on a personal computer. The input data were selected by comparing resonance profiles and characteristic patterns in the intensity data. The result of the fitting procedure is given in Table I. Only 12 series are given, resulting from the most prominent features of the spectrum. We do not find a single value for the ionization potential, but different values for each series, which can be sorted into several groups [see Fig. 2(a)]. This leads us to the conclusion, that angular momentum coupling in a pure Hund's case is no longer a valid description for HI in this energy range.

In Hund's case (c), good quantum numbers are only associated with $\mathbf{\Omega} = \mathbf{\Lambda} + \mathbf{\Sigma}$ ($\mathbf{\Lambda}$ is the projection of the total orbital electronic angular momentum and $\mathbf{\Sigma}$ that of the spin on the internuclear axis), and $\mathbf{J}'$ the total angular momentum. However, in our particular case, $\mathbf{\Lambda}$ is conserved to a good approximation as well as $\mathbf{l}$ and λ, the electronic angular momentum of the Rydberg electron and its projection on the molecular axis.

In Hund's case (e),[12] the molecule rotates as the ion core, and consequently, the good quantum numbers are now associated with $\mathbf{J}'$ and $\mathbf{J}^+$, the total angular momentum of the ion core, and $\mathbf{l}$ and $\mathbf{j} = \mathbf{l} + \mathbf{s}$ for the Rydberg electron. Series converging to a given rotational level of the ion core can now be defined. A scheme of the possible transitions in HI from the ground state to an excited state is given in Fig. 3.

To assign such Rydberg series, it is necessary to know the exact energy positions of the rotational levels belonging to the ionic core configurations $^2\Pi_{1/2}$ and $^2\Pi_{3/2}$. Unfortunately, the value of the $^2\Pi$ ionization potentials based on the data of Ref. 4 are not sufficiently precise. The values of Hart and Hepburn[8] did also not yield consistent results. Therefore, we had to assume some values for these limits. Taking into account the effect of the electric field at the threshold, we have used the value of 83 720 cm^{-1} for the $X\,^2\Pi_{3/2}$, $(J^+ = 3/2)$ limit.

Since the $A\,^2\Sigma^+ \rightarrow X\,^2\Pi$ emission spectrum has not been observed (probably because the A state is completely predissociated), no rotational data is known for the ground state of HI^+. By analogy with the other hydrogen halides, following a technique similar to Lempka *et al.*,[22] we have taken for B_0 a value of 6 cm^{-1} for the $X\,^2\Pi$ ionic ground state. The value of B_0 for the $X\,^1\Sigma^+$ ground state of HI is equal to 6.34 cm^{-1}.[23] The rotational energy of the different ionization limits is given by

$$B_0'(J^+ + \tfrac{1}{2})^2 \tag{2}$$

and therefore the difference in energy between $J^+ = 1/2$ and $J^+ = 3/2$ is $3\,B_0'$, while it is $5\,B_0'$ between $J^+ = 3/2$ and $J^+ = 5/2$. These ionization limits cannot explain the experimental results as can be seen from a comparison of Figs. 2(a) and 2(b).

It is now well established[14(a),15,24] that series with different l converge to levels of different parities. Therefore, it is important to introduce the Λ doubling of the $X\,^2\Pi_{1/2}$ state, the difference between the levels of e and f parity, which is, unfortunately, unknown experimentally. Using the formulas

$$\Delta\bar{\nu}_{fe} = p(J^+ + \tfrac{1}{2}) \tag{3}$$

and

$$p = \frac{4AB}{E_{\Pi} - E_{\Sigma}}, \tag{4}$$

where A and B are the spin–orbit and the rotational constant of the $X\,^2\Pi$ state, and E_Σ is the energy of the first $A\,^2\Sigma^+$ excited state, the splitting $\Delta\bar{\nu}_{fe}$ of the components with e and f parity of a rotational level can be calculated. Because $A < 0$

TABLE I. Results of the fitting procedure assuming Hund's case (c) angular momentum coupling. The input data for the nonlinear least-squares fit to Eq. (1) are given in the first two columns, labeled n and E_{obs}. The quantum defects given in μ_{obs} are calculated using the ionization potential IP (series limit), which, together with the mean quantum defect μ and the energy positions E_{fit}, is a result of the fit. The numbering of the series is organized from the energy of the lowest member observed for each series. The series number 1,2,3,4,6 correspond to the series V, I, II, III, and IV, respectively, of Refs. 4 and 8.

Series 1		IP: 89 123.4 ± 0.06 cm^{-1} μ: 0.4116 ± 0.000 04		Series 2		IP: 89 123.8 ± 0.3 cm^{-1} μ: 0.2762 ± 0.005	
n	E_{obs} (cm^{-1})	μ_{obs}	E_{fit} (cm^{-1})	n	E_{obs} (cm^{-1})	μ_{obs}	E_{fit} (cm^{-1})
6	85 611.0	0.4105	85 609.6	6	85 770.0	0.2799	85 774.3
7	86 592.7	0.4150	86 595.3	7	86 700.0	0.2714	86 696.5
8	87 215.1	0.4167	87 217.7	8	87 290.0	0.2643	87 284.3
9	87 639.7	0.3998	87 635.6	9	87 685.0	0.2668	87 681.9
10	87 930.0	0.4106	87 929.8	10	87 960.0	0.2897	87 963.2
11	88 141.0	0.4307	88 144.6	11	88 170.0	0.2739	88 169.6
12	88 305.4	0.4173	88 306.2	12	88 325.0	0.2794	88 325.4
13	88 434.1	0.3819	88 430.9	13	88 444.0	0.2949	88 446.0
				14	88 539.0	0.3018	88 541.2
				15	88 617.0	0.2855	88 617.6

Series 3		IP: 89 109.8 ± 0.2 cm^{-1} μ: 0.0354 ± 0.008		Series 4		IP: 89 134.6 ± 0.01 cm^{-1} μ: 0.0158 ± 0.0001	
n	E_{obs} (cm^{-1})	μ_{obs}	E_{fit} (cm^{-1})	n	E_{obs} (cm^{-1})	μ_{obs}	E_{fit} (cm^{-1})
6	86 024.1	0.0366	86 025.3	6	86 069.3	0.0168	86 070.2
7	86 848.6	0.0336	86 847.5	7	86 886.9	0.0128	86 884.9
8	87 382.1	0.0303	87 379.9	8	87 413.7	0.0145	87 413.2
9	87 744.5	0.0349	87 744.3	9	87 773.7	0.0204	87 775.0
10	88 003.3	0.0415	88 004.7	10	88 033.4	0.0175	88 033.8
11	88 195.4	0.0448	88 197.1				

Series 5		IP: 89 153.1 ± 0.08 cm^{-1} μ: 0.0182 ± 0.0001		Series 6		IP: 89 144.9 ± 0.3 cm^{-1} μ: 0.7521 ± 0.0008	
n	E_{obs} (cm^{-1})	μ_{obs}	E_{fit} (cm^{-1})	n	E_{obs} (cm^{-1})	μ_{obs}	E_{fit} (cm^{-1})
6	86 087.3	0.0172	86 086.2	7	86 323.9	0.7602	86 333.4
7	86 900.0	0.0211	86 901.9	8	87 066.7	0.7288	87 054.8
8	87 430.5	0.0185	87 430.6	9	87 541.7	0.72	87 530.2
9	87 792.2	0.0203	87 792.8	10	87 866.0	0.7712	87 859.9
10	88 052.7	0.0138	88 051.7	11	88 098.4	0.7471	88 097.9
11	88 244.7	0.009	88 243.2	12	88 273.0	0.7648	88 275.3
12	88 390.0	0.0082	88 388.7	13	88 404.0	0.8085	88 411.1
13	88 502.1	0.0167	88 501.9				
14	88 589.6	0.0450	88 591.8				

Series 7		IP: 89 113.4 ± 0.3 cm^{-1} μ: 0.2425 ± 0.0022		Series 8		IP: 89 113.0 ± 0.4 cm^{-1} μ: 0.0663 ± 0.0018	
n	E_{obs} (cm^{-1})	μ_{obs}	E_{fit} (cm^{-1})	n	E_{obs} (cm^{-1})	μ_{obs}	E_{fit} (cm^{-1})
10	87 960.0	0.2458	87 960.8	10	88 003.3	0.0556	88 000.9
11	88 166.8	0.2327	88 165.1	11	88 195.5	0.0637	88 195.1
12	88 318.5	0.2501	88 319.6	12	88 340.0	0.0852	88 342.5
				13	88 453.4	0.1011	88 457.0
14	88 534.0	0.2380	88 533.6	14	88 546.0	0.0882	88 547.8
15	88 611.2	0.2163	88 609.5	15	88 622.0	0.0502	88 620.9
16	88 671.0	0.2501	88 671.4	16	88 682.0	0.0435	88 680.8
17	88 721.0	0.2767	88 722.6	17	88 733.0	0.0065	88 730.3

TABLE I. (*continued*).

Series 9	IP: 89 134.6 ± 0.1 cm^{-1} μ: 0.1634 ± 0.0026			Series 10	IP: 89 115.2 ± 0.1 cm^{-1} μ: 0.8705 ± 0.0006		
n	E_{obs} (cm^{-1})	μ_{obs}	E_{fit} (cm^{-1})	n	E_{obs} (cm^{-1})	μ_{obs}	E_{fit} (cm^{-1})
12	88 350.0	0.1734	88 351.3	19	88 785.0	0.7696	88 781.3
13	88 470.0	0.1500	88 468.6	20	88 812.1	0.972	88 815.3
14	88 562.4	0.1507	88 561.4	21	88 843.6	0.8965	88 844.4
15	88 636.2	0.1614	88 636.1	22	88 867.9	0.9307	88 869.4
16	88 698.6	0.1349	88 697.0	23	88 892.0	0.8261	88 891.1
17	88 744.0	0.2381	88 747.5	24	88 909.8	0.8832	88 910.1
				25	88 927.2	0.8389	88 926.7

Series 11	IP: 89 118.9 ± 0.1 cm^{-1} μ: 0.5115 ± 0.0027			Series 12	IP: 89 125.4 ± 0.002 cm^{-1} μ: 0.5078 ± 0.0004		
n	E_{obs} (cm^{-1})	μ_{obs}	E_{fit} (cm^{-1})	n	E_{obs} (cm^{-1})	μ_{obs}	E_{fit} (cm^{-1})
19	88 799.2	0.4740	88 797.9	26	88 956.7	0.4993	88 956.6
20	88 828.7	0.5558	88 830.0	27	88 969.2	0.4963	88 969.1
21	88 857.4	0.5166	88 857.5	28	88 980.0	0.5337	88 980.2
22	88 881.3	0.5103	88 881.3	29	88 991.2	0.4082	88 990.3
23	88 903.0	0.4533	88 901.9	30	88 999.3	0.5061	88 999.3
24	88 919.2	0.5599	88 920.0	31	89 006.9	0.5728	89 007.4
25	88 936.1	0.4975	88 935.9	32	89 014.6	0.5369	89 014.8
26	88 949.5	0.5468	88 950.0	33	89 020.9	0.6022	89 021.5

($A = -5350\ \text{cm}^{-1}$), the coupling constant p as defined by Eq. (4) is positive.

Formula (4) is obtained in the pure precession approximation (p. 131 of Ref. 20). By comparison between the values obtained for the coupling constant p using this formula and the experimental values of HCl^+ and HBr^+,[25] a value for p corrected for the deviation from the pure precession is found to be equal to 3.5 cm^{-1}. The scheme of the different ionization limits is presented in Fig. 2(c).

From the fitting procedure it has been found, that the Rydberg series break off after 6–10 members, and a new series starts with a different set of constants. Only the highest

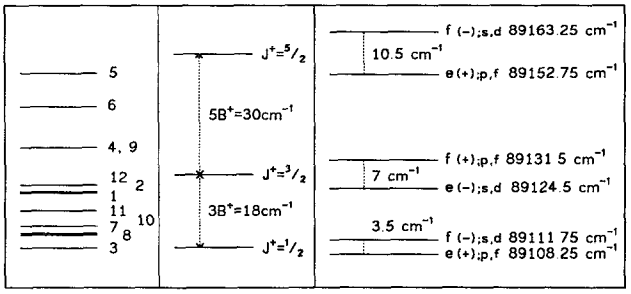

FIG. 2. (a) Results of the fitting procedure to a Hund's case (c) model. The different limits for each Rydberg series can be sorted into several groups. (b) The splitting of the different rotational levels $\mathbf{J}^+ = 1/2, 3/2, 5/2$ of the ion core in angular momentum coupling of Hund's case (e). (c) Calculated values for the different ionization potentials of the $^2\Pi_{1/2}$ state of the ion including the Λ-type doubling of the *e*- and *f*- parity components. Also given is the total parity (+ / −) of the final states. Due to the selection rules for the parity, different l waves are coupled differently to the parity components as shown in the figure.

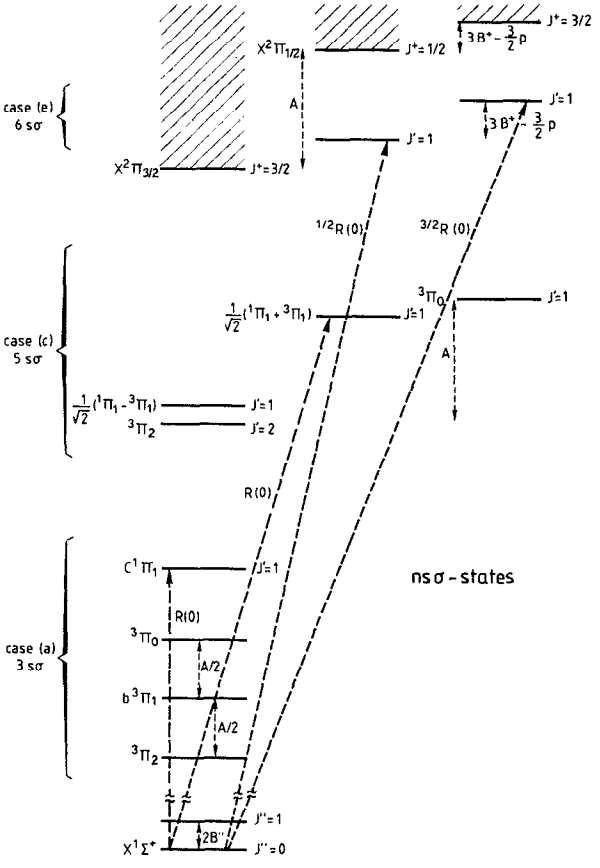

FIG. 3. Angular momentum coupling in HI demonstrated for the $ns\sigma$ states. The ground state and the lowest excited states couple in a Hund's case (a) model. The higher Rydberg states (e.g., $5s\sigma$) couple according to Hund's case (c). The Rydberg series converge to specific rotational levels $\mathbf{J}^+$ of the ionic $X\,^2\Pi_{1/2}$ state. Transitions from the ground state to rotational levels of the Rydberg states are also shown.

lying series (No. 12) extending from $n = 26$ to $n = 33$ should give a reasonable value for the associated series limit, in this case the e component of the $^2\Pi_{1/2}$, $\mathbf{J}^+ = 3/2$ limit at 89 124.5 cm^{-1}.

IV. THEORY

In this section, we describe how the coupling of the Rydberg electron changes from low values to large values of n. The MQDT is able to model any situation intermediate between two different coupling cases. The transition from Hund's case (b) to case (d) has been treated by Fano[13] using the geometrical frame transformation approach. In the case of HI discussed here, the transition goes from Hund's case (a) to case (c) and from case (c) to case (e). The geometrical frame transformation between the short range channels described in Hund's case (a), the channels described in Hund's case (c) and the long range ionization channels described in Hund's case (e) is introduced following the method outlined in Refs. 2 and 12. The effects of both spin–orbit and rotational autoionization are thus automatically taken into account for any value of n. The spin–orbit autoionization described in Hund's case (c) was discussed in Ref. 2 and the rotational autoionization described in Hund's case (e) is analogous to that appearing in Hund's case (d) (spinless situation) (for comparison, for H_2 see, e.g., Ref. 26). Due to the fact that there are different levels of the same total $\mathbf{J}'$ converging to the same or to different $\mathbf{J}^+$ limits, a residual electrostatic interaction perturbs the position of these levels. This interaction is a function of the difference between the quantum defects of the levels expressed in Hund's case (a) with same $\mathbf{l}$ but different λ and gives strongly varying values for the quantum defects along the series. For example, similar effects appear in the spectrum of the Rydberg levels of NO (Ref. 27, Fig. 11).

To understand the spectrum, we have now to consider a somewhat new spectroscopy: Usually from a $^1\Pi(J') \leftarrow X\,^1\Sigma^+(J'')$ transition, three rotational lines arise, one each in the P, Q, and R branch of the transition. When rotational mixing dominates, supplementary satellite lines appear due to the rotational mixing between triplets and singlets of the same $\mathbf{l}\lambda$ values (s uncoupling) and between singlets of same $\mathbf{l}$ but different λ (l uncoupling). For $\mathbf{l} \neq 0$, this situation is known for the case of Rydberg states converging to a Σ ionic core giving rise to $\mathbf{l}$ complexes (e.g., p complexes,[28] f complexes[29]). In our case, the situation becomes more complicated due to the mixing between triplets. Even for $\mathbf{l} = 0$, when $\mathbf{l}$ uncoupling is absent, it is not simple and can be illustrated as follows (see Fig. 3): For states with low values of n, Hund's case (a) is valid. Starting from $J'' = 0$, there is one $R(0)$ line corresponding to the transition $^1\Pi_1(J' = 1) \leftarrow X\,^1\Sigma^+(J'' = 0)$. When n increases, Hund's case (c) is obtained because the levels $^1\Pi_1$ and $^3\Pi_1$ are completely mixed by spin–orbit coupling. There is still an $R(0)$ line corresponding to the transition $1/\sqrt{2}(^1\Pi_1 + {}^3\Pi_1)(J' = 1) \leftarrow X\,^1\Sigma^+(J'' = 0)$, the final state being a member of a Rydberg series converging to the $X\,^2\Pi_{1/2}$ substate. When n is sufficiently large, this state becomes nearly degenerate with the $^3\Pi_0(J' = 1)$ level and Hund's case (e) is obtained with strong mixing between these two states by rotational coupling. The two resulting states, linear combinations of the three substates,[12] give rise to two Rydberg series with $R(0)$ lines only, one converging to $\mathbf{J}^+ = 1/2$ of $^2\Pi_{1/2}$, the other converging to $\mathbf{J}^+ = 3/2$ of $^2\Pi_{1/2}$. Using the notation[12]

$$^{\mathbf{J}^+ - J''}R(J''),$$

we have denoted the two Rydberg series as $^{1/2}R(0)$ and $^{3/2}R(0)$.

For $\mathbf{J}' = 2$, there are also two series, one converging to $\mathbf{J}^+ = 3/2$, the other converging to $\mathbf{J}^+ = 5/2$, denoted as $^{1/2}R(1)$ and $^{3/2}R(1)$. The energy interval between the lines of the two Rydberg series $^{3/2}R(0)$ and $^{1/2}R(1)$ which have the same limit becomes equal to $2B_0''$, the separation of the $J'' = 0$ and $J'' = 1$ sublevels of the ground state of HI, when n increases. The corresponding quantum defects converge to limiting values given by expressions of Hund's case (e) functions, as different linear combinations of Hund's case (a) functions. Due to perturbations between levels of the same $\mathbf{J}'$, deviations from this limit can be expected even for large values of n.

If $\mathbf{l} \neq 0$, the situation becomes more complicated. For $\mathbf{l} = 1$, there are five $R(0)$ lines and six $R(1)$ lines, for $\mathbf{l} = 2$, six $R(0)$ and nine $R(1)$ lines. These series have slightly different quantum defects and the intensity (and the widths) is spread out between the different lines. In conclusion, in Hund's case (e), $\mathbf{\Omega}^+$ of the core is defined, but ω the projection of $\mathbf{j}$ on the internuclear axis is no longer defined [see Eq. (2) of Ref. 12]. Therefore, there is j uncoupling for the Rydberg electron.

A program has been written, using the short range channels described in Hund's case (a) as a starting point and proceeding via a frame transformation as described in Ref. 12 to the long range ionization channels described in Hund's case (e). The MQDT system of equations is solved at each photon energy as explained for example in Ref. 30. The transition moments are weighted by the Hönl–London factors for case (a)–case (a) transitions and the rotational Boltzmann population corresponds to $T = 10$ K. The l mixing has been introduced only in the *ab initio* values of these transition moments, but neglected in the frame transformation. Consequently, the MQDT equations can be solved independently for each value of l and $\mathbf{J}'$. The photoionization cross section is obtained as a sum of all the cross sections in the $\mathbf{J}^+$ channels of the $^2\Pi_{3/2}$ substate open for each $R(J'')$ and $Q(J'')$ transition.

V. RESULTS OF THE CALCULATION

The spectrum is very sensitive to the values of the quantum defects. At first, we have used the *ab initio* quantum defects.[2] The results, obtained by the method described in the last paragraph, including only $R(0)$, $R(1)$, and $Q(1)$ lines for the s, p, and d series give already a qualitative agreement with the experiment. They are given for $11 \leqslant n \leqslant 15$ in Fig. 4, convoluted to a width of $\Delta\bar{\nu} = 1.0\,cm^{-1}$. For calculations made in pure Hund's case (c) or case (e) coupling, the

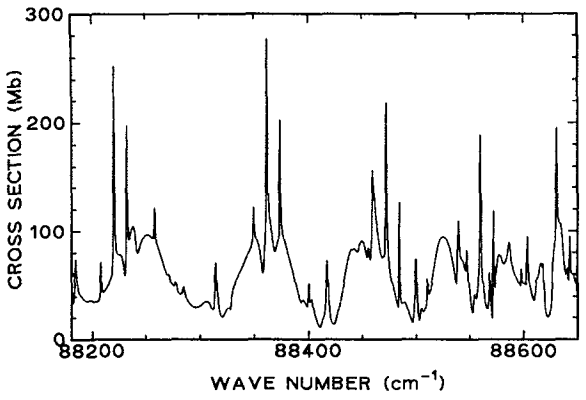

FIG. 4. Result of the calculation for $11 \leqslant n \leqslant 15$ using *ab initio* values for the quantum defects. There is only moderate agreement with the experimental results reproduced in Fig. 5(b).

resonances for different n are homothetic, e.g., except for a scaling factor they have the same shape, just like in an atomic Rydberg series. If the rotational autoionization is included by the MQDT calculation, the structures change when comparing n to $n+1$ due to the mixing between states of different Ω which changes for each value of n.

To obtain a better agreement with experiment, it is necessary to modify the initial quantum defects. Starting from the relations

$$\mu = \frac{\mu_0 + \mu_1}{2} \quad \text{and} \quad \mu_0 - \mu_1 = \frac{2}{\pi} \arctan\frac{1}{q} \tag{5}$$

and using the values of μ and q (the Fano index) from the experimental results for $n = 6$,[11] we have taken some trial values for the quantum defects of singlet (μ_0) and triplet (μ_1) states of the same Λ values. They are given in Table II together with the other quantum defects which have been estimated from calculations made for HCl.[31] In all the calculations we have used the *ab initio* transition moments. With this procedure, the absolute agreement with the experiment becomes better and permits tentative assignments to be proposed for the observed series (Table III). The results include the $R(0)$ lines for the f series and are given for $10 \leqslant n \leqslant 14$, in comparison with experimental data in Fig. 5. This region has been chosen, since it is well above the $^2\Pi_{3/2}$, $(v=2)$[32] (see Fig. 1) limit, and consequently not influenced by vibrational autoionization. A further classification of the series is given by the angular momentum of the Rydberg electron, denoted by j.

By following the $^{5/2}R(0), d, j = 5/2$ and $^{3/2}R(0), d, j = 3/2$ series through Fig. 5(a) it is illustrative to notice how the intensity of the individual members of these series change with n, causing effectively a reversal of the dominant contributing series of the spectrum. This change is repeated again in the series $^{3/2}R(0), d, j = 3/2$ and $^{1/2}R(0), d, j = 3/2$ at higher values of n. This last series can be autoionized in the $^2\Pi_{3/2}$ continuum ($J^+ \geqslant 3/2$) only by rotational autoionization and it has appreciable intensity only for $n \geqslant 18$. In this part of the spectrum, the latter series give only minor contributions. This reversal from one Rydberg series to another as the main contributor to the spectrum reflects quite well the structure observed in the experimental data for this spectral region. A major difference between experiment and theory is the intensity of the s series. The measured intensities are considerably smaller than calculated not only in this part of the spectrum, but also at low values of n. This problem was even more significant for the comparison with the first *ab initio* calculation without rotation.[2]

TABLE II. Quantum defects used in the calculation for the different states involved for $J' = 1$ and 2 ($J' = 1$ only for $l = 3$). For comparison, the *ab initio* values from Ref. 2 are given in parenthesis.

$l=0$	$^1\Pi$ $s\sigma$	$^3\Pi$ $s\sigma$								
	−0.04 (−0.1304)	0.04 (−0.0729)								
$l=1$	$^1\Pi$ $p\sigma$	$^3\Pi$ $p\sigma$	$^1\Sigma^+$ $p\pi$	$^3\Sigma^-$ $p\pi$	$^1\Delta$ $p\pi$	$^3\Delta$ $p\pi$	$^3\Sigma^+$ $p\pi$			
	0.449 (0.4630)	0.589 (0.4851)	0.355 (0.3157)	0.495 (0.4443)	0.55	0.6	0.7			
$l=2$	$^1\Pi$ $d\sigma$	$^3\Pi$ $d\sigma$	$^1\Sigma^+$ $d\pi$	$^3\Sigma^-$ $d\pi$	$^1\Delta$ $d\pi$	$^3\Delta$ $d\pi$	$^3\Sigma^+$ $d\pi$	$^1\Pi$ $d\delta$	$^3\Pi$ $d\delta$	$^3\Phi$ $d\delta$
	0.735 (0.6141)	0.809 (0.6659)	0.178 (0.0961)	0.334 (0.3926)	0.31	0.55	0.6	0.187 (0.0138)	0.405 (0.4797)	0.6
$l=3$	$^1\Pi$ $f\sigma$	$^3\Pi$ $f\sigma$	$^1\Sigma^+$ $f\pi$	$^3\Sigma^-$ $f\pi$	$^3\Delta$ $f\pi$	$^3\Sigma^+$ $f\pi$	$^1\Pi$ $f\delta$	$^3\Pi$ $f\delta$	$^3\Delta$ $f\varphi$	
	0.0864 (0.029)	0.0954 (0.0385)	0.0523 (0.0398)	0.1227 (−0.0014)	0.13	0.14	0.0656	0.076	0.001	

TABLE III. Results for the different rotational series derived by MQDT calculation. Assignments for the fitted series of Table I are proposed. In several cases, two of the fitted series correspond to a single rotational Rydberg series. When applicable, an assignment of further resonance structure to the theoretical results is given. These term values are denoted by *. For the series $R(1)$, the difference of $2B_0''$ (12.7 cm^{-1}) between the $J'' = 0$ and $J'' = 1$ levels has to be added before calculating the quantum defects.

n	E_{calc} (cm^{-1})	E_{obs} (cm^{-1})		($E_{obs} - E_{calc}$)	μ_{calc}	μ_{obs}
	Series $^{1/2}R(0)$, s			Limit = 89 111.75 cm^{-1}		
6	86 030.0	86 024.1	Series 3	− 5.9	0.033	0.038
7	86 853.0	86 848.6		− 4.4	0.030	0.037
8	87 386.0	87 382.1		− 3.9	0.026	0.035
9	87 750.0	87 744.5		− 5.5	0.023	0.041
10	88 010.0	88 003.3		− 6.7	0.020	0.050
11	88 202.0	88 195.4		− 6.6	0.017	0.057
12	88 347.5	88 340.0	Series 8	− 7.5	0.017	0.076
13	88 460.75	88 453.4		− 7.35	0.017	0.089
14	88 550.75	88 546.0		− 4.75	0.014	0.073
15	88 623.0	88 622.0		− 1.0	0.016	0.031
16	88 682.3	88 682.0		− 0.3	0.015	0.020
17	88 731.4	88 733.0		1.6	0.014	− 0.022
	Series $^{3/2}R(0)$, s			Limit = 89 124.5 cm^{-1}		
6	86 069.0	86 069.3	Series 4	0.3	0.007	0.007
7	86 878.0	86 886.9		8.9	0.011	− 0.003
8	87 404.0	87 413.7		9.7	0.014	− 0.009
9	87 764.5	87 773.7		9.2	0.017	− 0.013
10	88 023.0	88 033.4		10.4	0.019	− 0.029
11	88 214.0				0.022	
12	88 359.5	88 350.0	Series 9	− 9.5	0.023	0.097
13	88 472.75	88 470.0		− 2.75	0.024	0.051
14	88 562.75	88 562.4		− 0.35	0.023	0.028
15	88 635.25	88 636.2		0.95	0.023	0.009
16	88 694.5	88 698.6		4.1	0.025	− 0.052
17	88 743.6				0.026	
	Series $^{3/2}R(1)$, s^a			Limit = 89 163.25 cm^{-1}		
6	86 088.0	86 087.3	Series 5	− 0.7	0.014	0.015
7	86 900.0	86 900.0		0.0	0.017	0.017
8	87 427.5	87 430.5		2.5	0.020	0.013
9	87 787.0	87 792.2		5.2	0.029	− 0.021
10	88 048.5	88 052.7		4.2	0.021	0.002
11	88 240.0	88 244.7		4.7	0.022	− 0.007
12	88 385.5	88 390.0		4.5	0.023	− 0.012
13	88 498.75	88 502.1		3.35	0.025	− 0.059
14	88 588.75	88 589.6		0.85	0.024	0.013
15	88 661.1				0.026	
16	88 720.4				0.028	
	Series $^{3/2}R(0)$, p			Limit = 89 131.5 cm^{-1}		
7	86 595.0	86 592.7	Series 1	− 1.8	0.422	0.425
8	87 221.5	87 215.1		− 6.4	0.420	0.433
9	87 642.5	87 639.7		− 2.9	0.415	0.423
10	87 939.5	87 930.0		− 9.2	0.405	0.443
11	88 157.0	88 141.0		− 16.0	0.389	0.474

TABLE III. (*continued*).

n	E_{calc} (cm^{-1})	E_{obs} (cm^{-1})		$(E_{obs}-E_{calc})$	μ_{calc}	μ_{obs}
	Series $^{1/2}R(0)$, $d, j=3/2$			Limit = 89 111.75 cm^{-1}		
12	88 212.0				0.956	
13	88 366.5				0.865	
14	88 485.25	88 490.8	*	5.55	0.765	0.705
15	88 577.75	88 576.0	*	−1.75	0.665	0.688
16	88 650.5	88 646.0	*	−3.5	0.576	0.650
17	88 706.0				0.554	
18	88 749.1				0.605	
19	88 793.2	88 799.2	Series 11	6.0	0.439	0.262
20	88 821.8	88 828.7		6.9	0.546	0.310
21	88 852.3	88 857.4		5.1	0.434	0.229
22	88 876.8	88 881.3		4.5	0.388	0.178
23	88 899.7	88 903.0		3.3	0.251	0.072
24	88 915.3	88 919.2		3.9	0.365	0.127
25	88 930.9	88 936.1		5.2	0.367	0.005
26	88 945.9	88 949.5		3.6	0.277	0.006
27	88 958.1				0.275	
28	88 969.6				0.215	
	Series $^{3/2}R(0)$, $d, j=5/2$			Limit = 89 124.5 cm^{-1}		
7	86 323.0	86.323.9	Series 6	0.9	0.741	0.740
8	87 051.0	87 066.7		15.7	0.725	0.697
9	87 530.0	87 541.7		11.7	0.704	0.673
10	87 861.0	87 866.0		5.0	0.681	0.662
11	88 099.0	88 098.4		−0.6	0.655	0.659
12	88 276.0	88 273.0		−3.0	0.628	0.648
13	88 411.75	88 404.0	*	−7.5	0.594	0.659
14	88 518.0	88 518.0	*	0.0	0.549	0.549
15	88 603.0	88 602.0	*	−1.0	0.494	0.508
16	88 672.0	88 674.0	*	2.0	0.427	0.393
	Series $^{3/2}R(0)$, $d, j=3/2$					
7	86 511.0	86 515.0	*	4.0	0.520	0.515
8	87 173.0	87 193.7	*	20.7	0.501	0.461
9	87 615.0	87 622.5	*	7.5	0.474	0.452
10	87 925.0	87 917.4	*	−7.6	0.435	0.465
11	88 150.0	88 141.0	*	−9.0	0.388	0.437
12	88 313.5	88 318.5	Series 7	5.0	0.368	0.332
13	88 436.5				0.371	
14	88 533.5	88 534.0		0.5	0.379	0.368
15	88 610.5	88 611.2		0.7	0.388	0.378
16	88 675.1	88 671.0		−4.1	0.374	0.444
17	88 725.1	88 721.0		−4.1	0.424	0.509
18	88 768.7	88 785.0	Series 10	16.3	0.438	
19	88 808.2	88 812.1		3.9	0.373	
20	88 837.1	88 843.6		3.5	0.460	
21	88 867.3	88 867.9		0.6	0.344	
22	88 895.2	88 892.0		−3.2	0.123	
23	88 907.7	88 909.8		2.1	0.502	
	Series $^{5/2}R(0)$, $d, j=5/2$			Limit = 89 163.25 cm^{-1}		
6	85 767.0	85 770.0	Series 2	3.0	0.316	0.313
7	86 693.0	86 700.0		7.0	0.335	0.325
8	87 280.0	87 290.0		10.0	0.366	0.346
9	87 680.0	87 685.0		5.0	0.399	0.384
10	87 961.0	87 960.0		−1.0	0.446	0.450
11	88 169.0	88 170.0		1.0	0.494	0.489
12	88 327.5	88 325.0		−2.5	0.548	0.558
13	88 452.75	88 444.0		−8.75	0.572	0.648
14	88 551.75	88 539.0		−12.75	0.601	0.741
15	88 640.5	88 617.0		−23.5	0.511	0.826
16	88 709.6				0.446	
17	88 733.3				0.602	

TABLE III. (*continued*).

	Series $^{1/2}R(1)$, d,[a]			Limit = 89 124.5 cm^{-1}		
n	E_{calc} (cm^{-1})	E_{obs} (cm^{-1})		$(E_{obs} - E_{calc})$	μ_{calc}	μ_{obs}
7	86 437.0	86 436.9	*	− 0.1	0.595	0.595
8	87 112.0	87 109.9	*	− 2.1	0.592	0.596
9	87 563.0				0.583	
10	87 883.0				0.550	
11	88 131.0				0.422	
12	88 296.0	88 305.4	*	9.4	0.402	0.335
13	88 428.0	88 434.1	*	6.0	0.332	0.275
14	88 509.0	88 506.3	*	− 2.7	0.508	0.538
15	88 596.25	88 590.8	*	− 5.45	0.410	0.487
16	88 660.25	88 657.0	*	− 2.75	0.410	0.467

[a] Add 12.7 cm^{-1} before calculating the quantum defect.

Comparing the MQDT results given in Table III to the results of the fitting procedure of the experimental data given in Table I, a tentative assignment of the experimental data is proposed. A fitted series always corresponds to only a part of the theoretical results. In several cases, two fitted series combined can be assigned to one of the rotational series of the calculation. Whenever possible, an assignment of observed structure to the theoretical results is proposed. The remaining structures, not belonging to a fitted series, are denoted by an asterisk.

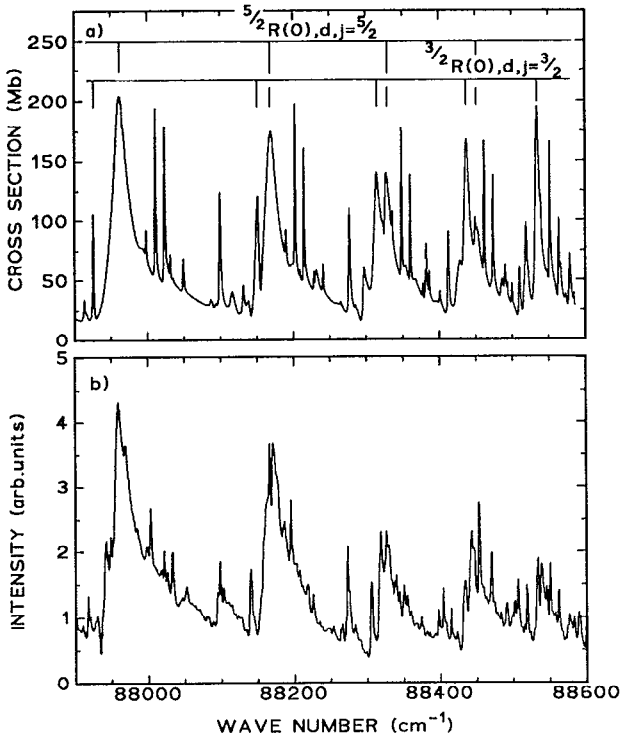

FIG. 5. Comparison of the theoretical results, using the empirical values for the quantum defects, with the experimental data for $10 \leqslant n \leqslant 14$. The calculated spectrum is convoluted to a resolution of $\Delta\bar{\nu} = 1.0\,cm^{-1}$. The assignments for the most prominent $R(0)$ transitions are indicated for the theoretical data in Fig. 5(a). For this calculation, the agreement with the experimental data is considerably improved as compared to the results Fig. 4. A comparison of the assignments obtained from theory and experiment is given in Table III.

To understand the effect of the perturbation between channels of different $\mathbf{J}^+$, we studied the d series for $\mathbf{J}' = 1$, including successively the different channels $(1/2 \leqslant \mathbf{J}^+ \leqslant 7/2)$. The $\mathbf{J}^+ = 1/2$ channel alone gives "atomic" Rydberg series with a nearly constant quantum defect. If the $\mathbf{J}^+ = 3/2$ channels are included, the levels converging to $\mathbf{J}^+ = 1/2$ and $\mathbf{J}^+ = 3/2$ interact together and are pushed from their initial positions to lower values by a quantity varying from 13 to 2 cm^{-1} when n goes from 14 to 17 [Fig. 6(a)]. The introduction of the channel $\mathbf{J}^+ = 7/2$ affects these levels again [Fig. 6(b)]. Due to the influence of these perturbations, the intensities and the widths of the peaks are changed. The intensities of the different channels are very different and depend strongly on the interference between the transition moments to $^1\Pi\ d\sigma$ and $d\delta$ and $^1\Sigma^+ d\pi$. For example, the series $^{7/2}R(0)$ has an intensity too small to appear in the figure.

Rotational perturbations become very drastic when the energy interval between n and $n+1$ becomes equal to the rotational energy. Coincidences between levels of same $\mathbf{J}'$, one with n and $\mathbf{J}^+ + 1$ and the other with $n+1$ and $\mathbf{J}^+$ can happen and give a perturbation. Although small (it varies as n^{-3}), this perturbation has a large effect on the quantum defect, resulting from the MQDT calculation as it is given in the sixth column of Table III, when n is large.

A better agreement with experiment could be obtained in principle if a nonlinear least-squares fitting procedure were used for all series at once. Such a procedure has been used for example for the Rydberg states of Li_2[33] with only four quantum defects to be determined. Here the number of different quantum defects (29 for $J \leqslant 2$) to be varied makes such an undertaking difficult, especially, since in addition the exact ionization limits are not known.

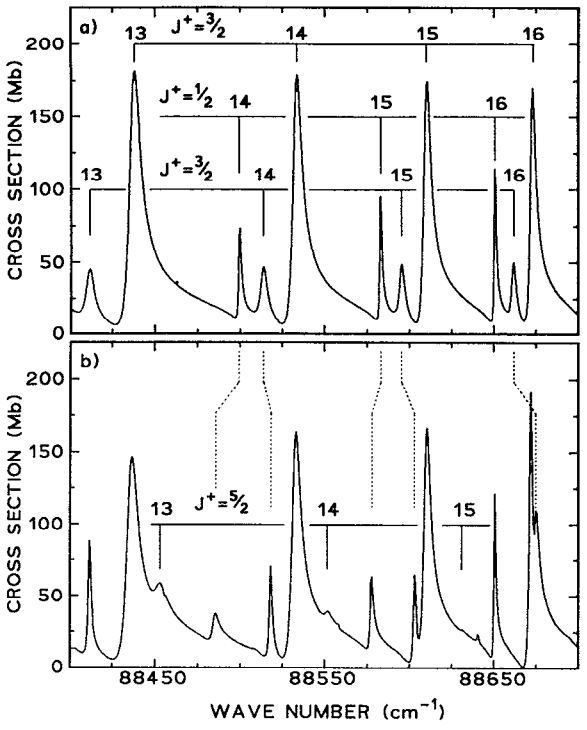

FIG. 6. Study of the perturbation between channels of different J^+. In Fig. 6(a), the results are given when only the $J^+ = 1/2$ and 3/2 channels are included. In Fig. 6(b) the effect of introducing in addition the channels $J^+ = 5/2$ and 7/2 is demonstrated. The lines are shifted and their intensities experience different alterations for each Rydberg member.

VI. CONCLUSION

We observed the photoelectron yield spectrum of the HI molecule in the spin–orbit autoionization regime with a spectral resolution high enough to resolve transitions between a rotational level of the ground state and one of the autoionizing state. Cooling the sample to a rotational temperature of 13 K simplified the spectrum to enable a detailed analysis of the rotational fine structure. A straight forward application of a least-squares fitting procedure for all members of the different Rydberg series leads to inconclusive results. However, the results of a MQDT treatment including molecular rotation are in good agreement with the experimental data, provided the angular momentum coupling is treated in terms of a transition from Hund's case (c) to Hund's case (e) coupling. The introduction of rotational autoionization and perturbations can alone explain the difference between successive Rydberg levels which is characteristic of the molecule. The effect of the vibrational autoionization which certainly affects the $n = 8$ and $n = 9$ levels could be taken into account as was done for HBr.[30] The results discussed here show that, without a MQDT analysis, assignments for the intensity structures are very difficult. Without a detailed analysis, it is difficult to try to understand details in the observed spin polarization parameters.[11] We hope that, in the near future, the ionization limits will be observed by rotationally resolved photoelectron spectroscopy[34] to give better values for the input data of the calculation.

ACKNOWLEDGMENTS

The authors want to thank G. Raseev and M. Büchner for stimulating discussions and Ch. Jungen for carefully reading of the manuscript. The experimental work was supported by the Deutsche Forschungsgemeinschaft in the SFB 216, and the collaboration between experiment and theory has been made possible by a grant of the European Community.

[1] C. H. Greene and Ch. Jungen, Adv. At. Mol. Phys. **21**, 51 (1985); G. Raseev, B. Leyh, and H. Lefebvre-Brion, Z. Phys. D. **2**, 319 (1986).
[2] H. Lefebvre-Brion, A. Giusti-Suzor, and G. Raseev, J. Chem. Phys. **83**, 1557 (1985).
[3] H. T. Wang, W. S. Felps, G. L. Findley, A. R. P. Rau, and S. P. McGlynn, J. Chem. Phys. **67**, 3940 (1977).
[4] J. H. D. Eland and J. Berkowitz, J. Chem. Phys. **67**, 5034 (1977).
[5] T. A. Carlson, P. Gerard, M. O. Krause, G. von Wald, J. W. Taylor, and F. A. Grimm, J. Chem. Phys. **84**, 4755 (1986).
[6] R. Hilbig and R. Wallenstein, IEEE J. Quantum Electron. **19**, 194 (1983); **19**, 1759 (1983); C. R. Vidal, in *Tunable Lasers*, edited by L. F. Mollenhauer and C. J. White (Springer, Berlin, 1987); P. R. Herman, P. E. La Rocque, R. H. Lipson, W. Jamroz, and B. P. Stoicheff, Can. J. Phys. **63**, 1581 (1985).
[7] T. Huth, A. Mank, N. Böwering, G. Schönhense, R. Wallenstein, and U. Heinzmann, in *Proceedings of the Fifteenth International Conference on the Physics of Electronic and Atomic Collisions, Brighton, United Kingdom, 1987, Invited Papers*, edited by H. B. Gilbody, W. R. Newell, F. H. Read, and A. C. H. Smith (Elsvier, New York, 1988), p. 607.
[8] D. J. Hart and J. W. Hepburn, Chem. Phys. **129**, 51 (1989).
[9] A. Mank, M. Drescher, T. Huth-Fehre, G. Schönhense, N. Böwering, and U. Heinzmann, J. Phys. B. **22**, L487 (1989).
[10] A. Mank, M. Drescher, T. Huth-Fehre, G. Schönhense, N. Böwering, and U. Heinzmann, J. Electron Spectrosc. **52**, 661 (1990).
[11] T. Huth-Fehre, A. Mank, M. Drescher, N. Böwering, and U. Heinzmann, Phys. Rev. Lett. **64**, 396 (1990).
[12] H. Lefebvre-Brion, J. Chem. Phys. **83**, 5898 (1990).
[13] U. Fano, Phys. Rev. A **2**, 353 (1970).
[14] J. Xie and R. N. Zare, Chem. Phys. Lett. **159**, 399 (1989); H. Lefebvre-Brion, *ibid.* **171**, 377 (1990); S. T. Pratt, J. L. Dehmer, and P. M. Dehmer, J. Chem. Phys. **93**, 3072 (1990); H. Frohlich, P. M. Guyon, and M. Glass-Maujean, *ibid.* **94**, 1102 (1991); K. S. Haber, E. Patsilinakou, Y. Jiang, and E. R. Grant, J. Chem. Phys. **94**, 3429 (1991).
[15] G. Raseev and N. A. Cherepkov, Phys. Rev. A **42**, 3948 (1990).
[16] M. Büchner, G. Raseev, and N. A. Cherepkov, J. Chem. Phys. (to be published).
[17] T. Huth-Fehre, A. Mank, M. Drescher, N. Böwering, and U. Heinzmann, Physica Scripta **41**, 454 (1990).
[18] U. Heinzmann, J. Phys. B **11**, 399 (1978).
[19] A. Mank, T. Huth-Fehre, M. Drescher, N. Böwering, and U. Heinzmann (to be published).
[20] H. Lefebvre-Brion and R. W. Field, *Perturbations in the Spectra of Diatomic Molecules* (Academic, Orlando, 1986).
[21] P. R. Bevington, *Data Reduction and Error Analysis for the Physical Sciences* (McGraw Hill, New York, 1969).
[22] H. J. Lemptka, T. R. Passmore, and W. C. Price, Proc. R. Soc. London, Ser. A **304**, 53 (1968).
[23] K. P. Huber and G. Herzberg, *Molecular Spectra and Molecular Structure IV: Constants of Diatomic Molecules* (Van Nostrand–Reinhold, New York, 1979).
[24] J. Xie and R. N. Zare, J. Chem. Phys. **93**, 3033 (1990).
[25] K. G. Lubic, D. Ray, D. C. Horde, L. Veseth, and R. J. Saykally, J. Mol. Spectrosc. **134**, 1 and 21 (1989).
[26] G. Herzberg and Ch. Jungen, J. Mol. Spectrosc. **41**, 425 (1972).
[27] S. Fredin, D. Gauyacq, M. Horani, Ch. Jungen, G. Lefevre, and F. Masnou-Seeuws, Mol. Phys. **60**, 825 (1987).
[28] J. W. C. Johns, in *Molecular Spectroscopy, Specialist Periodical Report*, edited by R. F. Barrow, D. A. Long, and D. J. Miller (Chemical Society, London 1974), Vol. 2, p. 513.
[29] Ch. Jungen and E. Miescher, Can. J. Phys. **47**, 1769 (1969).

[30] H. Lefebvre-Brion, P. M. Dehmer, and W. A. Chupka, J. Chem. Phys. **85**, 45 (1986).
[31] H. Lefebvre-Brion (unpublished calculations).
[32] N. Böwering, H. W. Klausing, M. Müller, M. Salzmann, and U. Heinzmann (to be published).
[33] M. Schwarz, R. Duchowicz, W. Demtröder, and Ch. Jungen, J. Chem. Phys. **89**, 5460 (1988).
[34] K. Müller-Dethlefs, M. Sander, and E. W. Schlag, Chem. Phys. Lett. **112**, 291 (1984); S. W. Allendorf, D. J. Leahy, D. C. Jacobs, and R. N. Zare, J. Chem. Phys. **91**, 2216 (1989).